III. EXPERIMENTAL APPARATUS

III.A. Introduction

A detailed description of the experimental apparatus used in experiments A and B is presented in this section. Additional information on the SLAC 8 GeV spectrometer facility may be found in the references describing earlier experiments[7, 29] which used this spectrometer.

III.B. Electron Beam and Charge Monitors

Electrons were accelerated to energies between 4.5 GeV and 18.0 GeV by the Stanford Linear Accelerator[30], which delivered a maximum of 360 pulses per second to the beam switchyard. The electrons were momentum analyzed, transported to End Station A, and focussed onto the target cells by the array of magnets and collimators shown in Figure (5).

Pulsed bending magnets PM1-PM5 deflected electrons 0.5 degrees to the quadrupole doublet Q10-Q11, which imaged the beam profile at the collimator C0 upon the energy-defining slits SL10. Two groups of four identical dipole magnets B10-B17 deflected the beam a total of 24 degrees; the first group dispersed the beam for momentum analysis at SL10. The quadrupole magnet Q12 insured that the beam was achromatic at the target position. The final focussing at the target was provided by the quadrupole doublet Q13-Q14. Horizontal and vertical vernier steering was obtained from a set of four dipole magnets.

The central energy and total energy spread of the electron
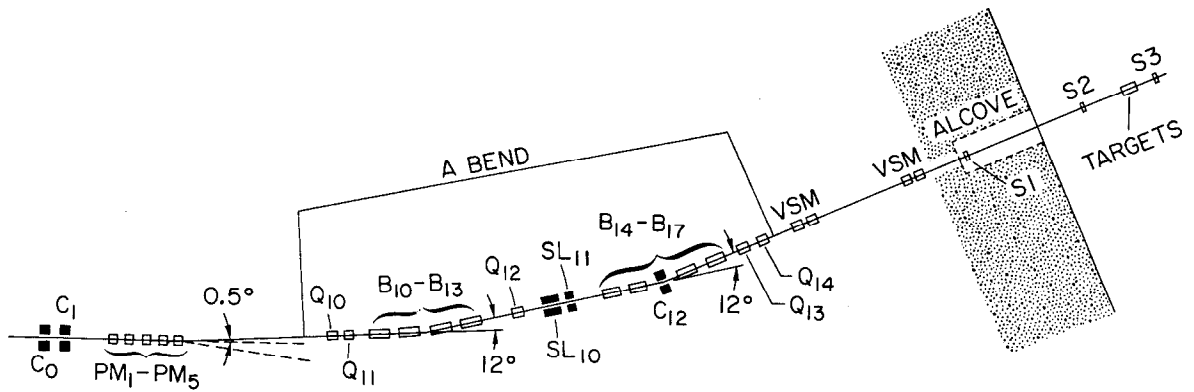
Fig. 5. Beam line configuration. Notation: B = main bend magnets; C = collimators; PM = pulsed bend magnets; Q = quadrupole magnets; SL = slits; S = fluorescent viewing screens; VSM = vernier steering magnets.

beam depended solely upon switchyard parameters and were independent of accelerator performance. Magnet currents in the series string of eight identical dipole magnets B10-B17 were set to the desired values after a standard degaussing cycle. Stability and repeatability of the fields of these magnets were monitored with a rotating-coil field probe located in a ninth identical dipole. This monitor magnet was connected in series with B10-B17, and the "flip-coil" measurements of its field provided a determination of the central beam energy to an absolute accuracy of $\pm$ 0.1%.[30] For each nominal energy the variations in the flip-coil measurements were well below this value. The horizontal opening of the slits SL10 determined the total energy spread of the electron beam. Except for some experimental runs in the resonance region (W < 2), a total spread in energy $\delta E/E$ of $\pm$0.25% was allowed. In the resonance region a total energy spread of $\pm$0.1% was used.

The beam halo generated at SL10 was reduced by the collimator C12, consisting of four moveable tungsten jaws followed by four associated ion chambers which monitored beam interactions in the jaws. At each change of incident energy, the four jaws were individually moved into the beam until the corresponding ion chamber indicated 50% of its trip level; the jaw was then moved back 2mm to prevent frequent beam trip-offs. Experimental runs using a 1/8" thick aluminum target with a 2" diameter hole about the beam centerline showed that singles rates in the

trigger counters due to beam halo could be reduced by better than a factor of two by using this method. As the distance between two aluminum flanges just above and below the liquid target cells was approximately two inches, these runs provided an estimate of the scattered electron yields from beam halo interactions with the target assembly. Such runs were made frequently at each incident energy, showing non-zero yields only at very low E', where the yields from hydrogen and deuterium are large.

The beam was aligned using the four vernier steering magnets and two zinc sulfide fluorescent screens (S1 and S2 in Figures 4 and 5), which were viewed by closed-circuit television monitors. These two screens were rolled out of the beamline after the beam was aligned, while a third screen (S3 in Figures 4 and 5) remained in the beamline downstream of the target position to monitor the beam steering and beam profile during the experimental runs. Another zinc sulfide screen included as part of the target assembly was frequently moved into the beam to examine the beam position and profile at the target position. Typically, the profile at the target was an ellipse 2mm high by 4mm wide. The uncertainty $\delta\theta$ in the incident electron direction from possible beam misalignment and divergence was ± 0.1 mrad, which is approximately 2/3 of the angular resolution of the 8 GeV spectrometer.

Two toroidal charge monitor systems[31] measured the incident charge per pulse and hence monitored the flux of elec-

trons impinging upon the target. The systems each used a ferrite-core toroid encircling the beam coupled directly to a precision capacitor. The waveform produced in this damped resonant circuit by the passage of the electron beam through the central hole in the toroid was amplified and sampled. The sampled signal was digitized and accumulated in a bi-directional accumulator which effectively averaged the noise component of the signal to zero. Each monitor was calibrated internally by discharging a precisely known pulse charge on to a single wire passing through the toroid. Ratios of measured charge to calibrated charge for runs of 10^4 pulses were always within 0.4% of unity. These internal calibrations were not used to provide an absolute calibration of the monitors, but rather served to monitor gain shifts in the individual monitor systems. The total charge accumulated by the toroid monitor just upstream of the target, when corrected for such gain shifts, gave the electron flux used in the cross section calculations. The two toroid monitors always agreed to 0.5% or better, and the random error in the flux measured for a run is believed to be $\pm$ 0.3%.

Both toroid monitors were periodically calibrated against a Faraday Cup[32] which could be moved into the beam at a position 13.5 meters downstream of the target position. Calibration runs were made at representative pulse charges, while pulse repetition rates were limited to 1 - 10 pulses per second.

Ratios of toroid to Faraday Cup measurements in these runs averaged to 0.998 $\pm$ 0.005. The results of the Faraday Cup calibrations indicated that the charge accumulated by the downstream toroid monitor gave the electron flux for a run with an absolute uncertainty of $\pm$ 0.5%.

Depending upon the counting rate at a given point, beam intensities ranging from 3×10^{10} to 5×10^{11} electrons/pulse were used. A lucite counter near the target served as a beam-spill monitor. Beam-spill traces viewed on an oscilloscope were kept reasonably flat-topped and had spill widths within the range 1.2 - 1.6 μsec. Spill width information as well as the total number of beam pulses was recorded for use in deadtime calculations[20] in the data analysis.

III.C. Targets and Density Monitors

The electron beam passed through target cells containing liquid hydrogen or liquid deuterium. As shown in Figure (6), the two cells were vertical cylinders which could be positioned by rotating the entire assembly about its vertical axis so that the beam traversed either cell along a diameter. The cell walls were made of 0.003 inch-thick aluminum for experiment A, and of 0.001 inch-thick stainless steel for experiment B. The length of liquid traversed by the beam was 6.95 cm for hydrogen and 7.12 cm for deuterium in experiment A, and 14.06 cm for hydrogen and 14.11 cm for deuterium in experiment B. Figure (6) shows the target assembly used in experiment B; it was only

HYDROGEN RESERVOIR

10 cm

DIRECTION OF
LIQUID FLOW

HYDROGEN
RESERVOIR

HEAT EXCHANGER

TACHOMETER

CIRCULATION FAN

FLOW

FILL AND
VENT LINE

UPPER VAPOR
BULB

BEAM

LIQUID TARGET
CELLS

LOWER VAPOR
BULB

FILL AND
VENT LINE

EMPTY TARGET
CELLS

ZINC SULPHIDE
SCREEN

HOLE TARGETS,
SOLID TARGETS

2722C30
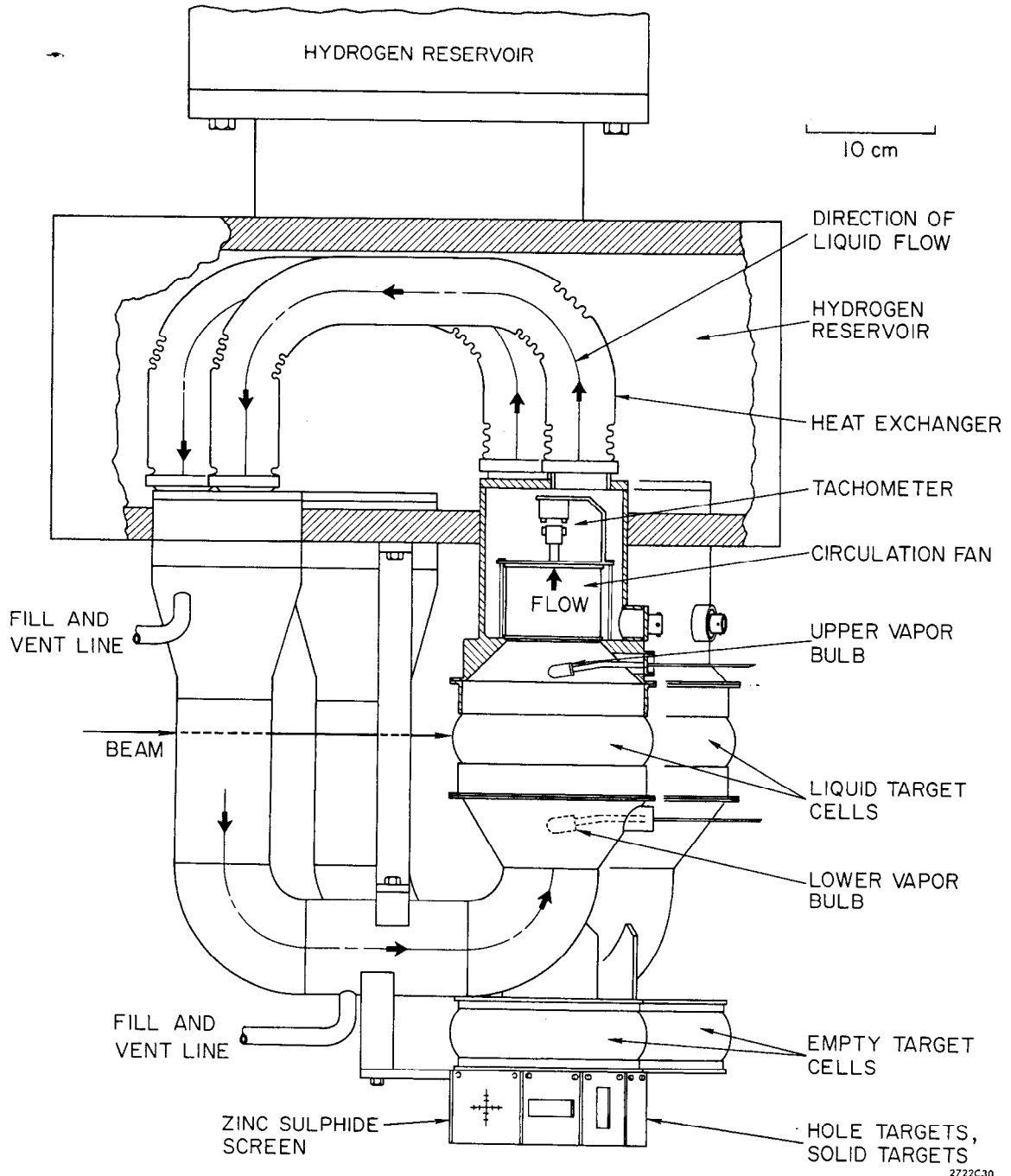
Fig. 6. Target configuration. The array shown here could be
rotated about a vertical axis and moved vertically to position
the targets available.

slightly different from that used in experiment A. Just
below each target cell was an empty replica target used for
determining cell-wall contributions to the measured cross
sections. Below these empty targets was an array of solid
targets, the targets having holes of various sizes, and the
zincsulfide screen. The entire assembly was suspended in
a scattering chamber maintained at 10^{-6} torr. It could
be quickly lifted, lowered, or rotated under computer control
to bring a specific target into the beamline at its proper
position.

Density changes in the liquid targets posed a formidable
obstacle that had to be overcome in order to use the high beam
currents available at SLAC. The hydrogen and deuterium tar-
gets were designed[33] to be cooled by forced convection
through closed loops, as shown schematically in Figure (6).
The upper half of each loop formed a heat exchanger in contact
with a reservoir of liquid hydrogen at 21° Kelvin. Natural
convection from beam heating, aided by an electrically driven
fan inside each loop, circulated the liquid and presented a
fresh segment of liquid to each beam pulse, obviating density
changes due to heating by the previous pulse. Test runs showed
that the measured scattering yield was independent of beam current
and pulse repetition rate (see also reference 29), provided
the fans were operating. The tachometer shown in Figure (6)
was added to each target for experiment B to give a positive
signal that each fan was functioning properly.

The primary target density monitor employed two hydrogen vapor pressure thermometers which indicated the target liquid temperatures above and below the beamline on each of the two target cells. A second density monitor employed the SLAC 1.6 GeV spectrometer[34] which, at each value of E, was set to detect recoil protons from elastic e-p or quasi-elastic e-d scattering at a fixed recoil-proton momentum and angle. With the target fans operating, the observed changes in the number of protons detected by the 1.6 GeV spectrometer per unit electron flux reflected the known target density changes as deduced from the small temperature drifts indicated by the upper vapor pressure thermometer. The hydrogen target fan operated properly for all the runs of the two experiments. The deuterium target fan operated properly except for runs at E = 8.6, 8.7, 10.4, 11.9, and 13.3 GeV in experiment A.

The target temperatures determined from the upper vapor pressure thermometer were used in the determination of the target densities for those runs in which the target fans were operating. Conversion tables for liquid temperature to density were readily available from cryogenic data.[35, 36] In addition, small corrections (∿0.2%) were applied[20] to account for the slow conversion of normal hydrogen to para-hydrogen[36], and for the small change in density resulting from the 1 atm over-pressure in the target cells. Similarly, corrections were made for small contaminations (∿1%) of HD in the deuterium targets.[20]

Data from the 1.6 GeV spectrometer were used in the de-
termination of the deuterium target density for those runs of
experiment A in which the deuterium target fan was not opera-
ting. No such data were available for runs at $\theta = 18^{\circ}$ and
E = 8.6 GeV, and no deuteron or neutron cross sections are
reported for that line. For each new value of E, normalization
runs were made at low beam currents ($\sim$3 ma) to ascertain the
yield of recoil protons per unit electron flux. Tests had
shown that the yield per incident electron at these low currents
was independent of whether the target fans were on or off,
indicating no significant density changes in the target liquid.[20]
Consequently, the density of the target in these normalization
runs could be ascertained from the temperature at the upper
vapor pressure thermometer. The 1.6 GeV spectrometer proton
yield per unit beam flux was then used to monitor the target
density in the remaining deuterium runs at that incident energy.
Depending upon the instantaneous beam current and repetition
rate, target density corrections of 1% - 30% were encountered
in those runs in which the deuterium target fan was not operating.
The uncertainty in these corrections is estimated to range from
0.4% to 0.6%.

Careful determination of target lengths and densities was
made primarily because the errors in those quantities do not
cancel in the ratio of deuterium to hydrogen cross sections and
therefore propagate into the error in σ_n/σ_p. Random errors in

the effective target density, arising mainly from fluctuations in the beam position and profile, were estimated to be 0.3% in both experiments. The hydrogen target densities were known to an accuracy of $\pm$ 0.7% in experiment A and $\pm$ 0.4% in experiment B, with the uncertainty attributable primarily to inaccuracies in the calibration of the vapor pressure thermometers and a $\pm$0.2% uncertainty in the cryogenic data for liquid hydrogen. Because the cryogenic data for deuterium are only quoted to an accuracy of $\pm$0.6%, the deuterium target density was known only to a level of $\pm$0.9% in experiment A (as long as the fan was operating) and $\pm$0.7% in experiment B. Target lengths were measured with micrometer calipers while the targets were warm and pressurized with air. Shrinkage of the targets when cooled to $21^{O}K$ was surveyed during experiment B, and its effects were included in the calculation of all target lengths. The target lengths were known to $\pm$ 0.6% in experiment A and $\pm$0.4% in experiment B. Samples of gas from the targets were analyzed for purity by mass spectrometry.

Experimental runs with empty replica target cells in the beam line were used to determine the target wall contributions to the measured cross sections. Substantial reductions in running time were realized by using a replica target which had 0.018" walls rather than the 0.003" aluminum walls of the liquid targets in experiment A, and 0.0075" walls rather than 0.001" stainless steel walls in experiment B. The extra thickness was selected

to simulate the radiative degradation of the electron energy in the full-target liquids.[37] After normalization by the ratio of cell-wall thicknesses, the empty-target background was typically 3-8% of the full-target yield in experiment A and 2-4% of the full-target yield in experiment B. The systematic uncertainty in the cross section from uncertainties in target cell wall thicknesses ranged from 0.1% to 0.6%.

III.D. Spectrometer

Scattered particles from the target cells were analyzed using the SLAC 8 GeV focussing spectrometer[38, 39, 40, 41] shown schematically in Figure (4). The three quadrupole magnets focussed point-to-point in the vertical plane and parallel-to-point in the horizontal plane. The horizontal production angle was displayed in the horizontal focal plane and momentum displayed in the vertical plane. The dipole magnets bent the optic axis a total of 30 degrees in the vertical plane. Scattered particles were delivered to a series of detectors located in a shielded cave just behind Q83. The entire assembly of magnets, detectors, and shielding was supported on a set of rails and could pivot about the target position to the desired scattering angles.

Magnet currents were adjusted under computer control to obtain the desired bending, dispersion, and focussing properties. Small corrections to the magnet currents, established in a series of optics tests[29] allowed the energy of the 8 GeV spectrometer

to be normalized to the beam switchyard value for the incident electron energy E. Elastic e-p scattering measured in both experiments indicated that the spectrometer value of E' of the elastically scattered electrons was within 0.05% of the expected value as calculated from E and θ, and this was taken to be the uncertainty in the calibration of E' versus E.

The spectrometer quadrupoles imaged the target at two focal planes located inside the shielded cave. The horizontal-angle, or theta, focal plane was oriented normal to the spectrometer central ray, while the vertical or momentum focal plane was oriented at an angle of 13.7°, as shown in Figure (7). Two scintillation counter arrays lying in each focal plane were used to determine the angle, θ, and momentum, P, of a scattered particle. The individual counters overlapped in separate rows to define 54 θ-bins and 20 P-bins.

Extensive measurements of the optical properties of the 8 GeV spectrometer were performed in November 1967 and are described in Kirk et al.(29) The detailed calculation of the spectrometer acceptance $\Delta\Omega\Delta P/P$ is presented in reference (26) and in Appendix I. The calculation used a TRANSPORT[38] model of the 8 GeV spectrometer (see Table XXII of Appendix I) incorporating measured excitation constants for the magnets. The transformation of charged particle coordinates from the target to the spectrometer focal planes is described by a matrix of first-and second-order coefficients in a Taylor series
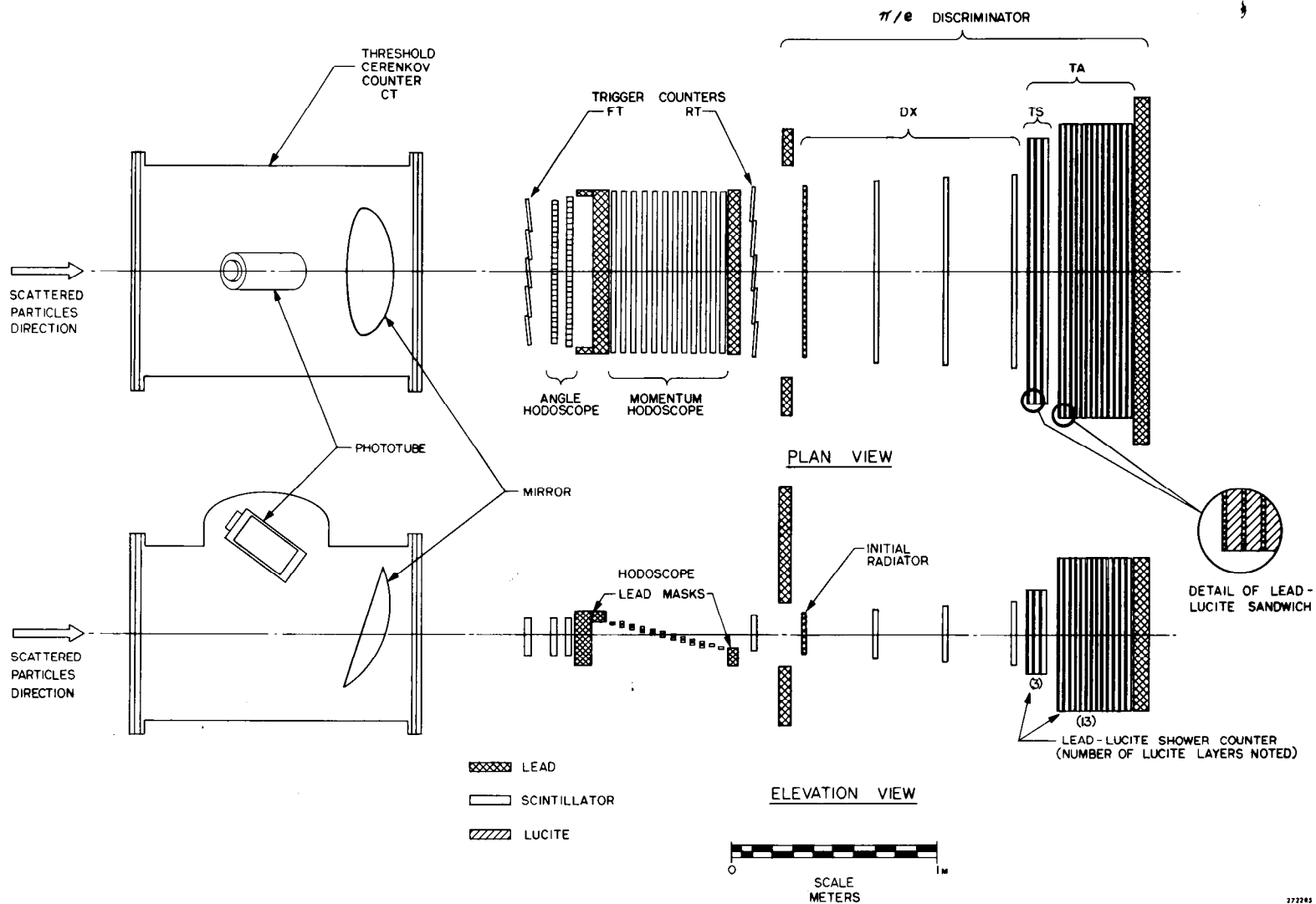
Fig. 7. Magnet focal plane detector arrays. Their positioning in the magnet spectrometer is shown in Fig. 4.

expansion of the particle coordinates about the spectrometer central ray. Using the matrix coefficients as described in Appendix 1, a Monte Carlo ray-tracing program was used to calculate the acceptance of the individual P-θ bins of the spectrometer focal planes. A P-θ bin is defined by the intersection of a P-bin and a θ-bin, so that ΔP and $\Delta\theta$ were already known from the measured P and θ dispersions. The azimuthal angular acceptance, $\Delta\phi$, for a particular P-θ bin averaged over the target length, was determined by lead apertures downstream of Q81 and B82 and ranged from ±12 mrad to ±30 mrad. The total acceptance $\Delta\Omega\Delta P/P$ summed over the 20 x 54 such P-θ bins was 2.833 millisteradian-percent; the theta hodoscope covered an angular range $\Delta\theta = \pm7.95$ mrad, while the momentum hodoscope accepted $\Delta P/P = \pm2.02\%$. In the off-line analysis of experiment B, all P-θ bins were used while in experiment A the hodoscope lead masks (see Figure (7)) partially shadowed the edge bins and events were accepted only if they fell within θ-bins 2-53 and P-bins 2-19. This restricted acceptance was 2.492 millisteradian-percent with $\Delta\theta = \pm7.65$ mrad and $\Delta P/P = \pm1.82\%$. The absolute uncertainty in either acceptance was believed to be about ±1.5%; an additional uncertainty of 1% due to a possible momentum dependence of the acceptance could not be ruled out. A list of the properties of the 8 GeV spectrometer is given in Table (I) along with estimates of the percentage uncertainties in these figures.

Table I. Properties of the 8 GeV Spectrometer

Property	Expt A	Expt B	% Error
Momentum resolution ($\delta P/P$)	± 0.10%	± 0.10%	1%
Momentum dispersion	2.91 cm/%	2.91 cm/%	1%
Momentum acceptance ($\Delta P/P$)	± 1.82%	± 2.02%	1%
Theta resolution	± 0.14 mrad	± 0.14 mrad	1%
Theta dispersion	4.58 cm/mrad	4.58 cm/mrad	1%
Theta acceptance	± 7.65 mrad	± 7.95 mrad	1%
Phi acceptance (max)	±29.6 mrad	±29.6 mrad	
Solid Angle ($\Delta\theta\Delta\phi$)	0.685 msr	0.701 msr	1.8%
Acceptance ($\Delta\theta\Delta\phi\Delta P/P$)	2.494 msr-%	2.833 msr-%	1.5%

III.E. Particle Detectors

III.E.1. Introduction

The particle detection system provided event triggers for essentially all the electrons scattered into the spectrometer acceptance and discriminated electrons from a background consisting predominantly of pions. All of the particle detectors, shown in Figure (7), were mounted on a steel boom tilted at 30 degrees to the horizontal. A concrete and lead cave shielded the detectors from backgrounds that would otherwise have swamped the true signals.

Scattered particles, after traversing the last quadrupole magnet, passed through a threshold Cerenkov (CT) counter filled with freon gas. They then traversed track-defining elements consisting of a front trigger (FT) counter followed by angle and momentum hodoscopes and a rear trigger (RT) counter. Next, a one-radiation-length lead slab serving as an initial radiator was followed by a group of three scintillation counters (DX), that measured specific ionization of the resultant particles. This slab was followed by fifteen additional one-radiation-length lead slabs interspersed with lucite that together formed the total absorption (TA) counter. The first three segments of the TA counter functioned as another detector, the truncated shower (TS) counter, sampling the early development of an electron shower.

All of the particle identification techniques exploited the fact that background particles had much larger rest masses than

electrons. The TA counter was used to define a good sample of electrons at all values of E', while the DX and TS counters gave additional pion rejection where needed. Particular emphasis in the following discussion is placed upon the functioning of each detector under conditions of high background rates, which were frequently encountered in the two experiments.

III.E.2. The Threshold Cerenkov Counter

The threshold Cerenkov counter, used to identify electrons, was 1.14 m long and was pressurized with gaseous Freon-12 (CCl_2F_2). It identified electrons by detecting the Cerenkov light emitted in the particle passage. A four-segment mirror reflected the Cerenkov light to a Phillips 58UVP phototube which viewed the interior of the counter through a quartz window. During experiment A, the gas pressure was maintained at 589 mm Hg, corresponding to a threshold for pions at E' = 3.5 GeV. During experiment B the gas pressure was maintained at 246 mm Hg corresponding to a threshold for pions E' = 5.5 GeV. Pions could still produce light in the counter by the production of secondary electrons, and consequently the CT counter was placed forward of all other detectors, to minimize the amount of material in the path of the particles. Events were accepted as electrons if sufficient Cerenkov light was produced in the counter. In experiment A we required that the anode signal from the phototube fire a discriminator circuit. In experiment B we required that the integrated charge from the anode pulse be above a minimum value.

Electrons fired the CT discriminator with an efficiency of 88.1 - 89.9% in experiment A with circuit deadtime corrections ranging from zero to two percent. This low efficiency was the result of a poor quality phototube and a misaligned mirror segment and poor optical coupling to the quartz window. This also resulted in a geometrical variation in the efficiency. Replacement of the phototube and re-alignment of the mirror system raised the electron detection efficiency to 98.0% in experiment B. This efficiency is believed known to better than 0.4% in both experiments. The Cerenkov counter discriminated against pions for $E' \lesssim 3.5$ GeV in experiment A and for $E' \lesssim 5.5$ GeV in experiment B. For energies below pion threshold, 0.3% to 0.7% of the background pions could still masquerade as electrons through the production of knock-on electrons and through chance coincidence.

III.E.3. Trigger Counters and Hodoscopes

The trigger counters and hodoscopes were located inside a light-tight, magnetically shielded box. The trigger counters were arranged in two rows of five scintillation counters, one row positioned near the entrance and one near the exit windows of the box. A "fast trigger" coincidence between any front trigger counter and any rear trigger counter was interpreted as the passage of a particle. Five counters were needed to cover the large horizontal acceptance and yet retain precise timing. In addition the substantial reduction in front and rear trigger deadtimes from the use of five counters allowed

operation at much higher trigger singles rates than would otherwise have been possible. The loss of events from trigger counter deadtimes was kept below 3%, and the trigger efficiency was essentially 100% in the limit of zero counting rate.

Each hodoscope consisted of two rows of scintillation counters with the back row offset by one half a counter width. A typical electron fired a counter in the front row and one or both of the two counters in the back row of each hodoscope that overlapped the one in front. The patterns of fired counters in each hodoscope were decoded to yield horizontal and vertical position, and hence the angle and momentum of a scattered particle. Reference (40) gives a very detailed description of the hodoscope decoding system procedure developed for the 8 GeV spectrometer. The adaptation of this procedure to our experiments[20] is summarized in section IV.A.

A new momentum hodoscope with 21 counters in two horizontal rows had been fashioned[26] for these experiments. The 20 momentum bins thus defined by the overlaps provided an rms resolution $\delta P/P \simeq \pm 0.1\%$. The theta hodoscope was the same one used in all previous experiments[7, 29] with the 8 GeV spectrometer. A total of 55 counters overlapped so as to define 54 θ bins with an rms angular resolution $\delta\theta = \pm 0.14$ mrad. The lead masks at the limits of both hodoscopes ensured that electrons falling outside the hodoscopes' edges would not shower in the total absorption counter.

III.E.4. <u>The π/e Discriminator</u>

The total absorption counter was composed of sixteen lucite slabs sandwiched between one-radiation-length lead slabs as shown in Figure (7). Each lucite slab was viewed by four RCA 6342-A phototubes; the anode signals from the 64 phototubes were added and the total signal pulse-height analyzed. For a single event this TA signal was proportional to the shower multiplicity and, consequently, to the electron's energy. A typical spectrum had a pion peak in low channels and a roughly gaussian electron peak whose position was proportional to E' and whose fractional full-width at half maximum (FWHM) varied roughly according to $(E')^{-1/2}$. A cut placed one FWHM below the peak center divided events into two classes. Electrons fell into the upper class with 99.1% frequency; the lower class was discarded as background. Systematic uncertainty in the total absorption counter efficiency was about $\pm 0.2\%$.

The pion peak had an exponential tail attributable mainly to pion-nucleus interactions in the TA counter. This tail typically extended to high channels, making difficult a clean separation of electrons from background. At high E', near pion-electroproduction threshold, where pion rates were low and the electron peak fell in very high channels, separation was straightforward. At lower E', large pion background began to obscure the electron peak and the CT counter had to be used in addition to the TA counter to provide the needed pion rejection. At the very lowest E' where electrons com-

prised less than 1% of all detected particles and the electron
peak was in low channels good signatures in the DX or TS count-
er were also needed to discern an electron peak. For detection
of positrons (i.e., for positive spectrometer polarity) the
full array of counters was usually required to give adequate
rejection of backgrounds.

The DX counters, individually pulse-height analyzed, were
used to determine whether a shower had begun in the initial
radiator. In general, a pion would traverse the initial radiator
without interaction and would register in each counter as a
single-ionizing particle, with a typical Landau distribution.
With probability about 70%, an electron would produce fast
secondary particles that enhanced the anode signals from each
counter. The pulse-height spectrum of a single DX counter
for an electron sample showed a Landau peak in low channels
followed by a broad continuum corresponding to production of
one or more fast particles. A cut placed in the valley be-
tween the Landau peak and this continuum, corresponding to
a signal about 1.5 times that of a single minimum ionizing
particle, insured moderate insensitivity to gain shifts. The
DX condition required an event to have signals above this
cut in all three DX counters or it was considered background.
The pion rejection of the threefold DX counter was about 97%,
while the efficiency for single electrons[26] varied from
60.9% at E' = 2 GeV to 80.5% at 8 GeV. A second cut at 2.5
times minimum-ionizing pulse height gave better than 99% pion

rejection, but the electron detection efficiency fell to 38.3%
at 2 GeV and 65.0% at 8 GeV.

A correlation between the observed DX efficiency and the
background singles rates was a potentially serious source of
error, as these rates were different for deuterium and hydrogen
targets. This correlation arose because chance coincidence
with background particles enhanced the observed pulse height
and correspondingly enhanced the apparent electron-detection
efficiency of the DX system. This enhancement was typically 1-2%
in kinetic regions where the DX counter was needed, but was
as high as 5% in some very high-rate runs. A rough parameteriza-
tion[26] of the enhancement was obtained using the fast
trigger and DX singles rates. When the base DX efficiency
was corrected using this function, the systematic uncertainty
in the DX efficiency was less than 0.5%.

Another counter that sampled the early shower development
was the truncated shower (TS) counter. Anode signals from the
first three lucite slabs were picked off and summed to produce
the TS signal which was independently pulse-height analyzed.
A typical TS spectrum for pions showed a peak in the lowest
few channels with a greatly foreshortened exponential tail.
Electrons registered as a Poisson-distributed peak centered
about a pulse height that was roughly proportional to E'.
In the analysis of experiment A, a variable cut placed in the
valley between the electron and pion peaks insured a 90.1%
efficiency for detection of electrons. In the analysis of

experiment B, two different fixed cuts were used in a manner similar to the treatment of the DX counter. Electrons produced a TS signal above the low cut with an efficiency that ranged from 90.1% at E' = 3.0 GeV to 97.8% at E' = 8.0 GeV. Similarly, the electron detection efficiency using the high cut ranged from 72.5% at E' = 3 GeV to 93.0% at E' = 8 GeV. Uncertainties in these efficiencies were less than $\pm$0.3%.

The TS counter condition was always used before the DX counter when both were available to reject backgrounds. The TS counter was much more effective in domains where the singles rates were high. As the counter elements were lucite instead of scintillator, additional soft background particles made little difference, and no rate-dependence of the efficiency was observed. The TS counter also proved to be superior to the DX counter in general, as two simultaneous pions produced a signal that was usually below the cut in the TS spectrum. There were some runs in which extremely large backgrounds required the use of both the DX and TS counters. Because the two counters both sampled the early shower development, and the DX and TA signals were correlated for a given event, their electron-detection efficiencies were not independent. In those runs an electron-detection efficiency was used[26] for the TS counter that accounted for this correlation.

III.F. Data Logging

Anode signals were routed from the detectors to the count-

ing house and converted by fast logic into digital information.
This trigger logic generated an interrupt to an SDS 9300 com-
puter for every likely event and provided digital information
about the response of the detectors. The event interrupt di-
rected the computer to scan buffers for the information deposite
there by the event logic; this information was written onto
magnetic tape for later analysis.

The event interrupt to the computer was derived from the
anode signals of the front and rear trigger trigger counters
and the CT or TA counters. Signals from the ten trigger counter
were independently discriminated and fed to two logical OR
circuits, as shown in Figure (8). A coincidence between
any front trigger and any rear trigger produced a fast trigger
or C1. The fast trigger in time with a pulse from either
the CT or TA discriminators formed two definitions (C2 and C9)
of a likely electron event. The TA discriminator output sig-
nal by itself provided a backup definition of a likely elec-
tron event, independent of C1 circuit deadtime losses. Thus
the event trigger circuit OR4 was virtually 100% efficient
for electron events. The output of OR4 set a latch-type flip-
flop circuit which was reset only by the accelerator pretrigger
just prior to the next beam pulse. This flip-flop set transi-
tion in turn generated the hardware interrupt to the computer;
only one such interrupt could be generated per beam pulse be-
cause the computer could not handle a faster event rate. The
output of OR4 was redundantly scaled to allow accurate cor-
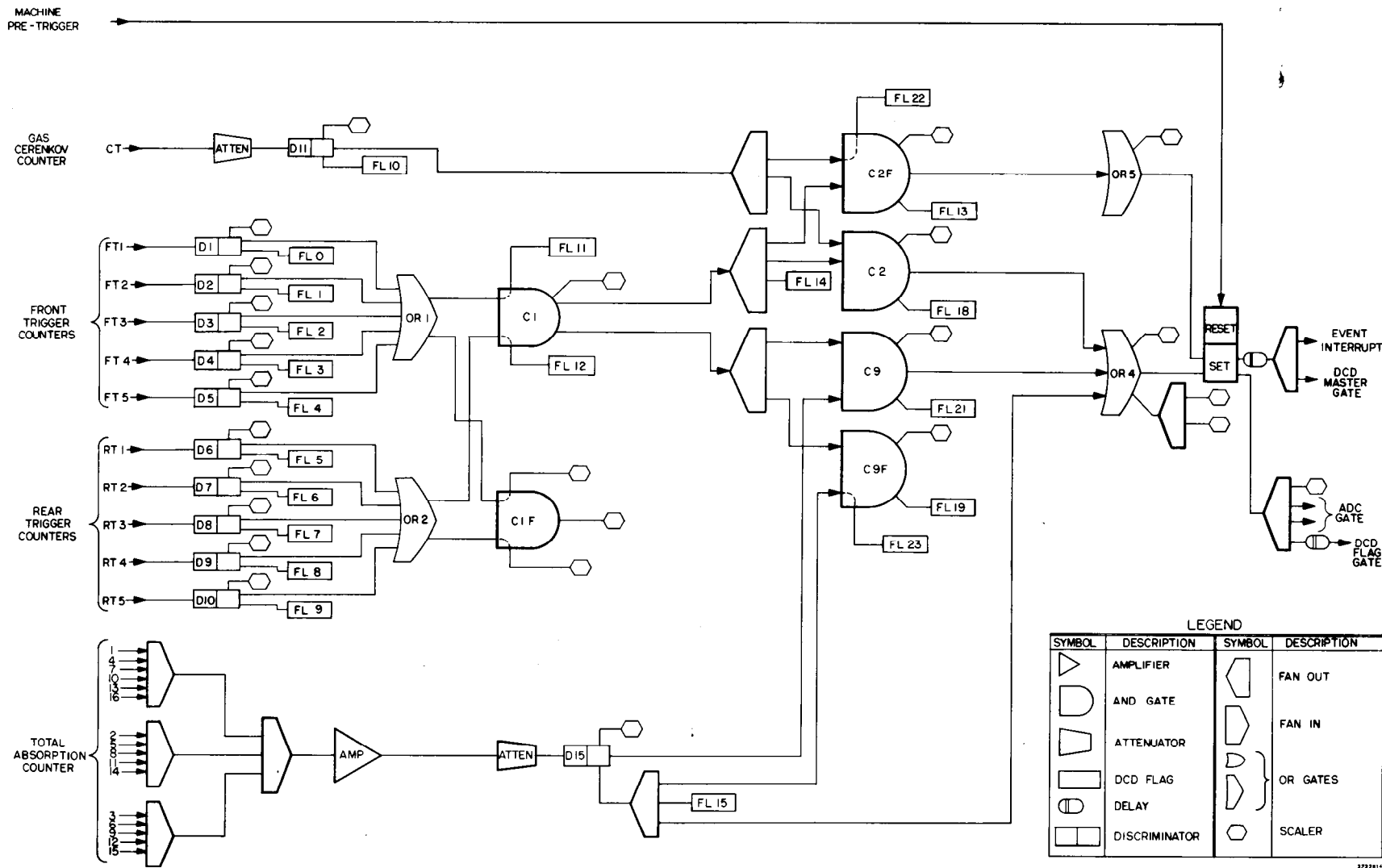
Fig. 8. The fast electronic logic. This array developed the main Event Interrupt to the computer and the master gate pulse to the Discriminator – Coincidence – Discriminator (DCD) units associated with the hodoscope counters.

rections for the "computer deadtime". Event rates were kept

below 0.5 events/pulse by adjusting the beam current; this

corresponded to a maximum 25% loss of events. The threshold

on the TA discriminator was set to minimize the number of pion

triggers while ensuring 100% efficiency for electrons. Below

E' = 2 GeV, however, between 1% and 10% of the electrons would

fail to fire this circuit, and a high efficiency for triggering

on electron events could be maintained only with the help of the

C2 coincidence trigger. The chance coincidence contribution

to the event triggers was monitored by false coincidence cir-

cuits C2F and C9F, which were parallel to the trigger circuits

C9 and C2.

Binary characteristics of each event were flagged by DCD

(Discriminator-Coincidence-Discriminator) circuits, which timed

output signals from the various descriminators and coincidence

circuits against gate pulses from the trigger logic. A success-

ful coincidence set a flip-flop that was read by computer via

multiplexer interface. The pattern of hodoscope counter events

was recorded in much the same manner. An event pulse also trig-

gered linear gate and stretcher circuits that processed the

pulses from the TA, CT, DX, and TS counters prior to conversion

by a bank of six analog-to-digital converters (ADC's) whose

digitized information was read by computer.

The SDS 9300 Computer[41], with 32K 24-bit words of

core storage, logged the data onto magnetic tape for later analy-

sis. Twelve words of information were written onto magnetic tape

for each event. These data included 76 bits for the θ and P hodo-
scope counters, 32 bits for DCD flags, the outputs of the six
ADC's, two target temperature readings, and the beam pulse charge.

In addition to logging events, the computer performed many
tasks that were invaluable to the successful execution of the
experiment. An on-line analysis of a sample of the events was
carried out by the computer. It was extremely helpful in detect-
ing and diagnosing equipment malfunction. Oscilloscope displays
of pulse-height spectra and related histograms provided in-
formation about the performance of the apparatus, both in
the end station and the counting house. Between runs, appro-
priate targets were positioned into the beam and magnet cur-
rents set to desired levels using feedback loops under com-
puter control. Experimental runs were started and stopped
with the aid of the computer, which logged scalers and
charge monitors at the end of a run and cleared them at the
beginning. During a run, when it was not logging events,
the computer monitored magnet currents, target temperatures, and
the voltages of all photomultipliers and electronics power
supplies.